IEEE Open Journal of
Antennas and Propagation

Received 13 December 2020; revised 10 January 2021; accepted 11 January 2021. Date of publication 16 February 2021; date of current version 24 March 2021.

Digital Object Identifier 10.1109/OJAP.2021.3059471

Design of a Cylindrical Crossed Dipole Phased Array Antenna for Weather Surveillance Radars

MOHAMMAD-HOSSEIN GOLBON-HAGHIGHI [1] (Member, IEEE), MIRHAMED MIRMOZAFARI [1] (Member, IEEE), HADI SAEIDI-MANESH [1] (Member, IEEE), AND GUIFU ZHANG [2] (Senior Member, IEEE)

[1] Advanced Radar Research Center, University of Oklahoma, Norman, OK 73072, USA

[2] School of Meteorology, Advanced Radar Research Center, University of Oklahoma, Norman, OK 73072, USA

CORRESPONDING AUTHOR: M.-H. GOLBON-HAGHIGHI (e-mail: golbon@ou.edu)

This work was supported by the National Oceanic and Atmospheric Administration under Grant NA11OAR4320072 and Grant NA16OAR4320115.

ABSTRACT We present a cylindrical dual-polarization phased array antenna for weather surveillance radars that features high isolation, matched copolar beams, low sidelobe levels, and adaptive null steering. We present a crossed dipole antenna element to replace the patch antenna on the currently deployed cylindrical polarimetric phased array radar (CPPAR). The crossed dipole element offers suppressed surface wave and lower coupling between adjacent elements of an array. As a result, we achieved lower backlobe and sidelobe levels, and a higher match between copolar beams of CPPAR compared to the currently deployed multi-layer patch antenna. Further reduction of the sidelobe level and adaptive null steering are obtained using a modified particle swarm optimization. The proposed null steering mitigates the interference among the four concurrent beams of a cylindrical phased array radar. The improvement in CPPAR radiation characteristics has been verified by comparing the presented crossed dipole antenna's radiation patterns and the existing aperture coupled patch antenna. The proposed crossed dipole phased array can benefit national weather radar networks to provide accurate multiparameter measurements enabling reliable observation of severe weather phenomena.

INDEX TERMS Pattern synthesis, particle swarm optimization, radiation pattern, phased array radar.

I. INTRODUCTION

MULTIFUNCTION Phased Array Radar (MPAR) investigates the feasibility of a shared radar system to replace the weather surveillance, terminal weather, and air-traffic control radars [1]–[3]. MPAR offers significant cost savings and efficiency in operation. The mechanically rotating weather surveillance radar (WSR-88D) requires about five minutes to complete a volumetric scan. This is too slow to observe the detailed evolution of severe weather phenomena. To do so, the national weather radar network requires a fast volumetric scanning of about one minute. In addition, weather observations impose stringent requirements on the polarimetric radiation patterns. For instance, to distinguish rain from melting snow, the error of the copolar correlation coefficient, ρ_{hv}, must be less than 0.01 [4]–[5]. This can be translated as a higher than %99 resemblance between horizontal and vertical copolarization patterns. Moreover, the intrinsic differential reflectivity, Z_{DR}, ranges from 0.2 dB for dry snow to 4 dB for large raindrops. To obtain the precision of 0.2 dB, the antenna should have cross-polarization isolation of better than 40 dB within the entire scanning.

To fulfill the requirements for MPAR, we proposed and prototyped a cylindrical polarimetric phased array radar (CPPAR) [2], [3], [6]. The conceptual drawing of the CPPAR is shown in Fig. 1. The electronically scanning of the volume with four concurrent beams provides a rapid data update compared to conventional mechanical scan radars [7]–[10]. CPPAR circumvents most of the shortcomings of the planar polarimetric phased array antenna. Rather than scanning with a planar aperture, CPPAR commutates azimuthally providing scan-invariant beams in azimuth direction and high polarization purity [1].

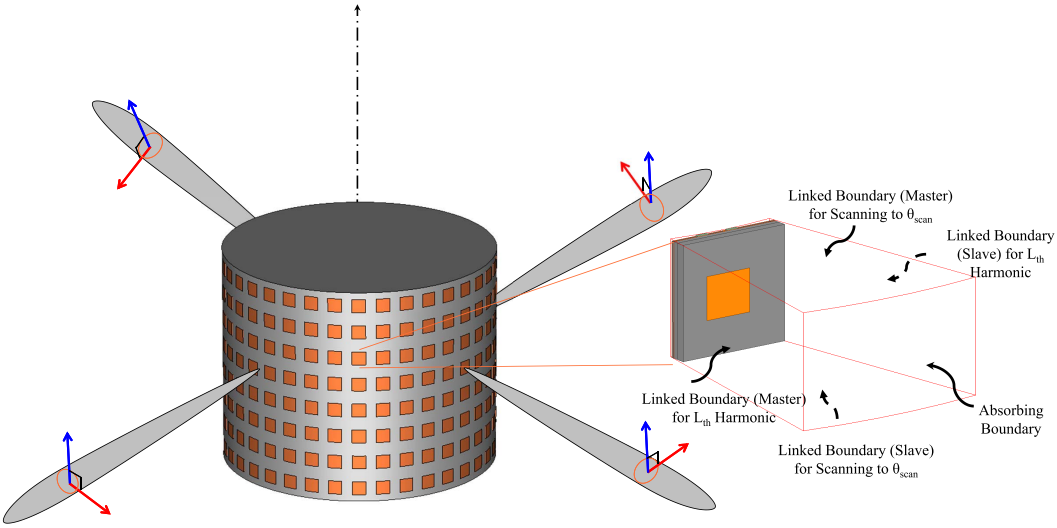

FIGURE 1. CPPAR schematic along with the unit cell illustration in HFSS for obtaining the patch antenna active element pattern in a cylindrical array.

We fabricated and characterized the CPPAR demonstrator, as shown in Fig. 1, with 2m diameter at the Advanced Radar Research Center (ARRC) of the University of Oklahoma [7]. The CPPAR demonstrator, though beneficial as proof of concept, seems to have room for further modifications. For instance, CPPAR ideally is supposed to have four independent sectors. However, the four beams of the CPPAR with relatively high side and backlobes may destructively interfere. This is due to strong surface wave excitation on the continuous grounded dielectric of the cylinder that results in a significant coupling between elements. Different natures of these couplings for horizontal and vertical polarizations manifest themselves as a mismatch between copolar beams of two polarizations. Finally, the coupling between elements deteriorates the polarization purity of the array antenna. These drawbacks necessitate revisiting the antenna structure on CPPAR to enhance its polarimetric performance.

This article proposes a cylindrical polarimetric phased array using a new antenna structure with enhanced polarimetric performance. We designed a crossed dipole as an element for CPPAR to replace the currently deployed multilayer patch antennas. The proposed crossed dipole does not require a thick substrate over the ground plane. Therefore, reduced mutual coupling between adjacent elements and lower sidelobes are achieved owing to surface wave suppression. The cylindrical active element pattern for the proposed crossed dipole is accurate calculated using phase mode analysis. Then, this active element pattern is used in a modified particle swarm pattern optimization. An adaptive null steering technique is proposed to mitigate the interference among four concurrent scanning beams of CPPAR. To do so, we adjust the nulls of a beam, right in the main beam directions of adjacent quadrants. Other goals of the optimization are to achieve the desired sidelobe levels (SLL), beam-width (BW), and matched copolar radiation patterns. The implemented optimization method is modified by an iterative particle swapping feature to improve computational efficiency and increase the convergence rate for the proposed multi-objective optimization. In addition to CPPAR, we will investigate radiation characteristics for larger cylindrical arrays with 5m and 10m diameter, technically called Terminal-MPAR (TMPAR) and MPAR, respectively.

II. PROPOSED CROSSED DIPOLE AND ITS CYLINDRICAL ACTIVE ELEMENT PATTERN

One of the main objectives of this research is to introduce a new element and demonstrate its enhanced radiation performance over the existing CPPAR element. In doing so, we first analyze the cylindrical active element pattern of the currently deployed patch antenna. CPPAR demonstrator is a 2m diameter cylindrical array which is populated by 96 columns of 19-element series-fed patch antenna shown in Fig. 1 [11]. To cover the required frequency range of MPAR, 2.7 to 2.9 GHz, a stacked patch structure is utilized as an element [11]. This structure includes seven layers for feedlines, apertures, and radiating patches. Such thick grounded substrate creates a proper medium that can support various modes of circumferential surface waves [12]–[13]. As these modes propagate around the cylinder, they radiate and diffract from the edges. This can be observed as some ripples near the broadside direction in the active element pattern of the cylindrical array [13], [14]. Therefore, the CPPAR active element pattern can be considered as a means to investigate surface wave excitation around the cylinder. To obtain the cylindrical active element pattern (E_{AEP}), we adopt phase mode analysis in conjunction with HFSS master/slave boundary condition capability [14]–[15]. Eq. (1) defines a periodic cylindrical active element pattern as the sum of N harmonics, where N is the number of elements around the cylinder and θ is the elevation angle in which the active element pattern

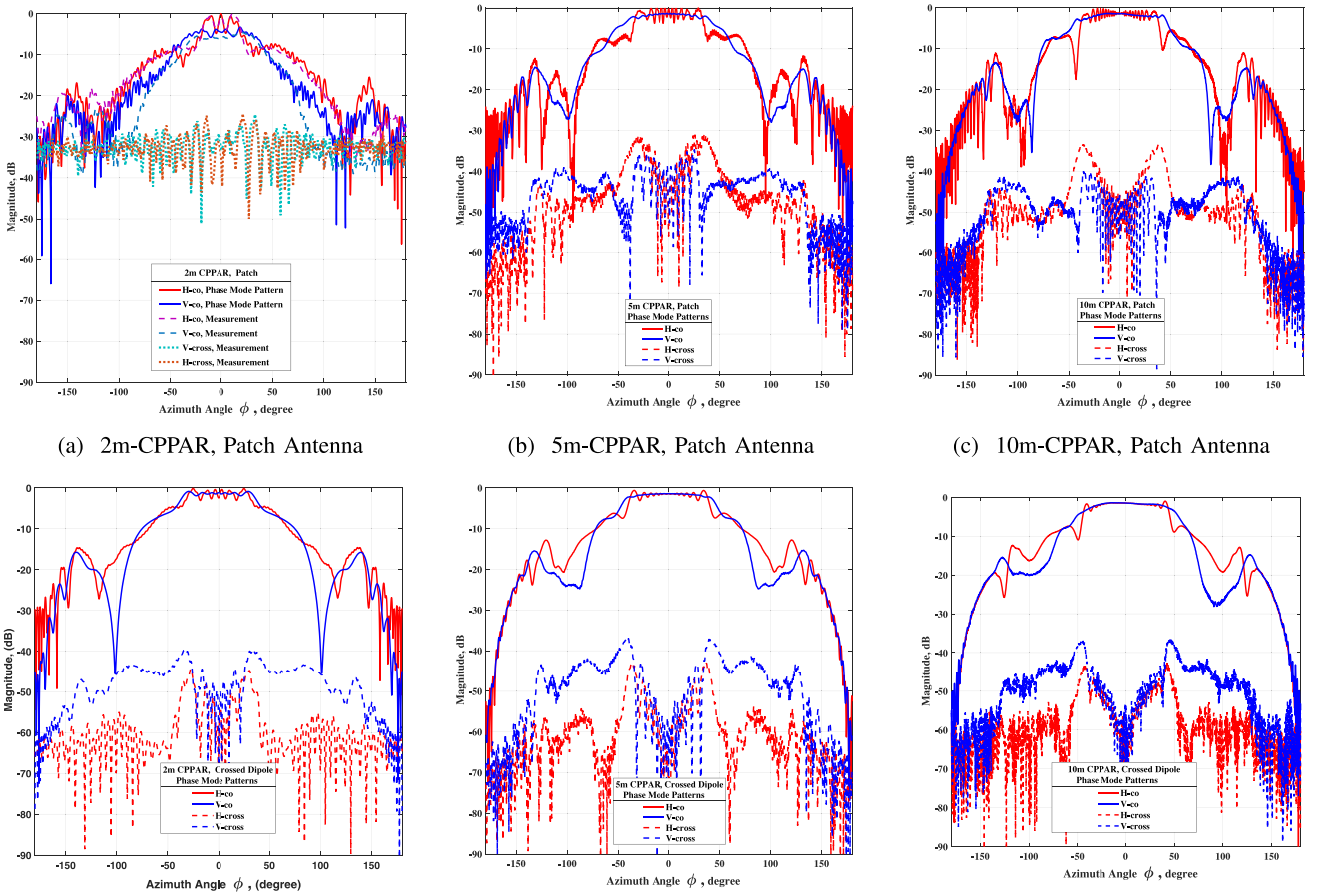

(a) 2m-CPPAR, Patch Antenna (b) 5m-CPPAR, Patch Antenna (c) 10m-CPPAR, Patch Antenna

(d) 2m-CPPAR, Crossed Dipole Antenna (e) 5m-CPPAR, Crossed Dipole Antenna (f) 10m-CPPAR, Crossed Dipole Antenna

FIGURE 2. **CPPAR measured and simulated embedded element patterns.**

is calculated.

$$E_{AEP}(\theta,\varphi) = \frac{1}{N}\sum_{l=0}^{N-1} E^{l}(\theta,\varphi) \tag{1}$$

According to Eq. (1), each of these harmonics, $E^{l}(\theta,\varphi)$, can be treated as a linked boundary condition (master/slave) in a FEM solver (HFSS) whose corresponding problem is shown in the subset of Fig. 1.

$$E^{l}(\theta,\varphi) = \sum_{n=0}^{N-1} E^{l}_{HFSS}\left(\theta,\varphi - n\frac{2\pi}{N}\right)e^{j\frac{2\pi}{N}nl} \tag{2}$$

The N far-field components of the HFSS unit cell, $E^{l}_{HFSS}(\theta,\varphi)$, can be treated as N independent problems. These are simultaneously simulated saving a great amount of computation time. Then these far-field components are extracted, post-processed according to Eq. (2), and added to obtain the cylindrical active element pattern. The above-mentioned steps for the currently deployed patch antenna were carried out for the 2m-CPPAR, 5m-CPPAR, and 10m-CPPAR, and their corresponding active element patterns are provided in Fig. 2a, Fig. 2b and Fig. 2c, respectively.

The CPPAR active element patterns have been measured in-situ, and the experiment environment is illustrated in Fig. 3. The measurement results, in Fig. 2a, verify the above-mentioned phase mode analysis to extract the active element patterns of large cylindrical arrays. As observed, there are some undesired features in the active element pattern of the patch antenna, which is due to its intrinsic properties. The multi-layers patch antenna having a thick grounded dielectric supports various surface modes propagating around the cylinder and diffracting from discontinuities [13], [14]. As a result, we observe high cross-polarization, side, and back lobe levels. The coupling mechanisms and surface wave excitations are not similar for both polarizations of the patch antenna. In an array of rectangular patch antennas, the horizontal radiating slots are located in close proximity, facing one another. This causes a strong coupling between elements resulting in a strong surface wave excitation for horizontal polarization. Therefore, we observe a mismatch between vertical and horizontal copolar patterns in Fig. 2a close to broadside direction. This mismatch between two radiation patterns increases the correlation coefficient, which adversely affects the polarimetric performance.

FIGURE 3. CPPAR in-situ experiment environment.

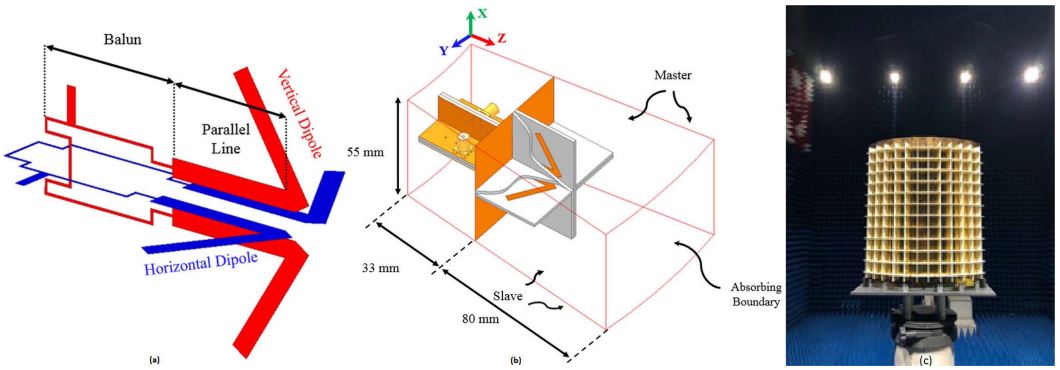

FIGURE 4. Proposed crossed dipole structure. (a) Conceptual drawing of the antenna, (b) Physical implementation and the corresponding unit cell illustration (Parts of the substrates are removed to disclose the bent dipoles in between.), (c) crossed dipole antenna.

To address the above-mentioned failures of the currently deployed patch antenna, we propose a crossed dipole antenna shown in Fig. 4. The proposed dipole stands a quarter wavelength above the ground plane, eliminating the need for a grounded continuous substrate. This way, we substantially suppress the higher-order modes of the surface wave [12], [16], which is reflected in the reduced ripples of the crossed dipole coplanar patterns, as shown in Fig. 2d. Moreover, we designed identical radiation elements for two polarizations. As seen in Fig. 4a, two radiation elements have similar dipoles, parallel lines, and half-wavelength baluns. The crossed dipole is center-excited as opposed to patch antenna having an offset excitation [16], [17]. As a result, we obtained an enhanced match between copolar patterns of the crossed dipole, which gets better as the radius of the cylinder increases. Fig. 4a shows the fabricated cylindrical array of the proposed cross-dipole antenna. The antenna elements are soldered to the ground planes. Each column is accurately mounted on the fixture to create a cylindrical array. We have measured the reflection coefficient and cross coupling of a middle element and compare them with simulation results in Fig. 5. The measured reflection coefficients of both polarizations are below -14 dB across the entire bandwidth, showing a well matched antenna to 50-ohm impedance. Also, the isolation between horizontal and vertical polarizations is better than 56 dB. Comparing to prior proposed antennas with the same polarimetric application [18], [19], we have achieved higher isolation between two polarizations [20].

Figs. 2d, 2e, and 2f demonstrate a significantly enhanced match between copolar patterns of the proposed crossed dipole compared to those of the patch antenna on the 2m-CPPAR, 5m-CPPAR, and 10m-CPPAR. The other considerable enhancement is the backlobe reduction of the crossed dipole active element patterns. This is achieved due to suppressed surface waves and reduced coupling between the proposed crossed dipole elements. For its balun implementation, we used stripline structures with two sub-ground planes on both sides of each balun, along with a row of surrounding metalized vias. This cavity-shaped structure considerably reduces the balun to balun coupling between adjacent elements. Comparing to those of the patch antenna, we achieve about 17 dB and 5 dB backlobe reductions for vertical and horizontal polarizations, respectively. Finally, the baluns are hidden below the principal ground planes and attached to dipoles through crossed slots cut in the ground plane. This way, the parasitic radiations of the baluns are blocked by the ground plane, leaving the array with pure radiations of the dipoles. Using such a technique, we have significantly reduced the cross-polarization level of the cylindrical array. Compared to aperture coupled patch antenna, more than 15 dB cross-polarization reduction is achieved using the crossed dipole antenna. This gives rise to significant enhancement in differential reflectivity (Z_{DR}) of the polarimetric performance.

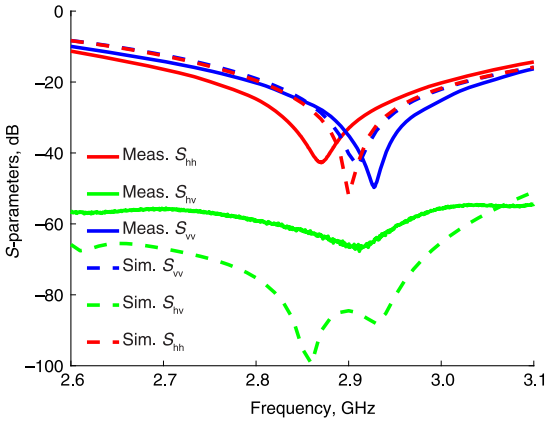

FIGURE 5. Simulated and measured reflection coefficients and isolation between the horizontal and vertical polarizations.

III. CYLINDRICAL ARRAY RADIATION PATTERN AND PROPOSED OPTIMIZATION METHOD

A modified PSO algorithm is proposed to optimize the beamforming weights of CPPAR antennas by minimizing the interference between adjacent beams and achieve a radiation pattern with the desired SLLs, beamwidth, and matched copolar patterns. The array radiation pattern of CPPAR in $(\theta_0\ ,\ \varphi_0)$ direction can be calculated as: [21]–[23]

$$E(\theta,\varphi)=\sum_{m=1}^{M}\sum_{n=1}^{N}\{w(n,m)f_{n,m}(\theta,\varphi)\times\exp\{+jk((r\sin(\theta)\cos(\varphi-n\Delta\varphi)+z_m\cos(\theta))\}\times\exp\{-jk((r\sin(\theta_0)\cos(\varphi_0-n\Delta\varphi)+z_m\cos(\theta_0))\}\} \quad (3)$$

where N is the total number of elements around the cylinder and M is the total number of elements along the axis of the cylinder, $\varphi_n=\Delta\varphi$, and z_m are the location of elements on the cylindrical coordinate system, r is the radius of the cylinder, $w(n,m)$ is the complex beamforming weights, $f_{n,m}(\theta,\varphi)=E_{AEP}(\theta,\varphi-n\Delta\varphi)$ are the rotated active element patterns with respect to elements' locations on the circumference of the cylinder.

Having this framework, we optimize the beamforming weights (i.e., $w(n,m)$) using the modified particle swarm optimization (MPSO) to achieve the above-mentioned goals. Several iterative/evolutionary optimization algorithms have been previously proposed for beamforming optimization [21], [23]–[28]. PSO is an evolutionary optimization method that can obtain an acceptable solution for non-convex optimization problems. PSO simulates bird flocking behaviors [25], [26], [29]–[32]. A group of birds, as social animals, is randomly searching for food. For our case, the complex beamforming weights (w) are considered as particles, in which both amplitude ($|w|$) and phase ($\angle w$) needs to be optimized. While the amplitudes of beamforming weights basically contribute to achieve desired SLLs and BWs, the adaptive null steering is mainly controlled by the phase of beamforming weights. Mask is defined as the desired radiation pattern, and the distance of the radiation patterns to the mask is considered as the distance of PSO particles to the optimal value.

In the PSO, the best strategy to find the optimal value is to follow the best particle, which has the nearest position to the optimal value. The PSO uses a learning / iterative technique to update the beamforming weights to solve the optimization problem. The optimization starts by initializing the beamforming weights, as the PSO particles, with semi-random values. Deterministic distributions such as Taylor or Chebyshev distributions can be used as the initial guess to increase the convergence rate of the optimization. In each step, each beamforming weight is scored based on how well that weight solves the problem by calculating the distance of its array pattern to the mask. The beamforming weights then updated in the solution space by using an advanced method. Then, the beamforming weights are scored again in their new states [21], [25], [26].

The optimization problem is defined for our case to obtain sidelobe levels less than a desired mask, steering the nulls right in the main beam directions of adjacent quadrants, and matching the copolar patterns for all beams. Therefore, in the n^{th} iteration, the position of the k^{th} particle is updated as:

$$p_{n+1}^{k}=p_{n}^{k}+v_{n}^{k} \quad (4)$$

where p_n^k stands for the position of the k^{th} particle at the n^{th} iteration. The new location of each particle is obtained from their current position and velocity of the particle. The velocity of each particle is updated as:

$$v_{n+1}^{k}=\omega v_{n}^{k}+\varphi_1 r_{n+1}\left(p_{n}^{k}\{\text{local best}\}-p_{n}^{k}\right)+\varphi_2 r_{n+1}\left(p_{n}^{k}\{\text{global best}\}-p_{n}^{k}\right) \quad (5)$$

where ω is Inertia or Momentum; v_n^k is the current velocity of the k^{th} particle; φ_1, φ_2 are correction factors; r_{n+1} is a random values between [0, 1]; $p_n^k\{\text{local best}\}$ is the best position of the k^{th} particle at the n^{th} iteration, and $p_n^k\{\text{global best}\}$ is the best position of all particles.

The pattern synthesis for the CPPAR is a non-convex problem, and thus, some of the particles may fall into local optima and never converge to the global optimal value. Hence, we proposed an adaptive particle swapping technique to improve the convergence rate. This feature is utilized to replace the particles with the farthest distance to the optimal value after a specific number of iterations. These particles could not be converged within an acceptable range from the optimal value during the optimization and need to be replaced by new particles. New particles are randomly distributed in the solution space with the mean equal to the global best position. This feature can improve the optimization performance by increasing the convergence rate, especially for multi-objective optimization problems.

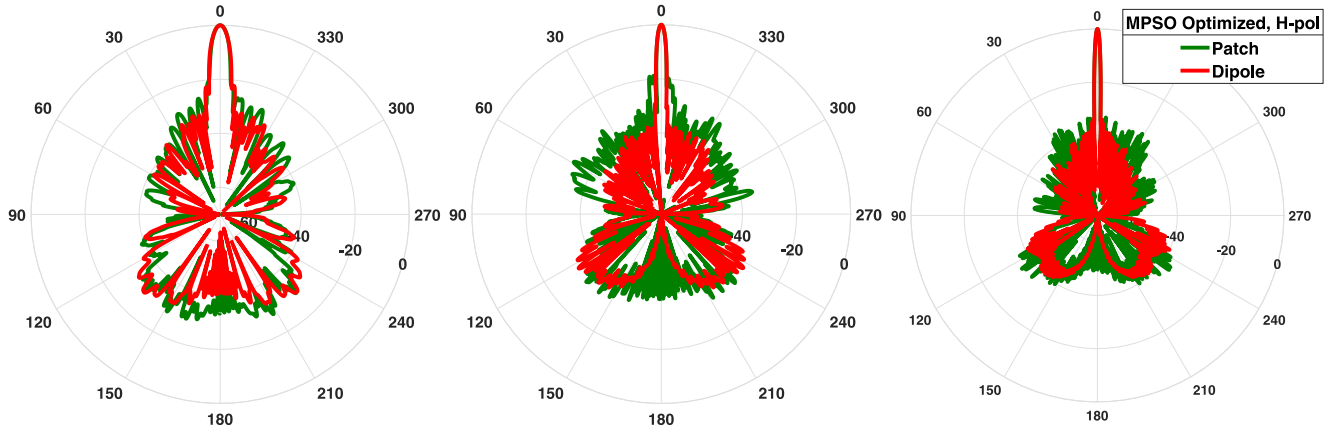

(a) 2m-CPPAR (b) 5m-CPPAR (c) 10m-CPPAR

FIGURE 6. Optimized radiation patterns for horizontal polarization using crossed dipole and patch elements for a) 2m-CPPAR, b) 5m-CPPAR, and c) 10m-CPPAR.

IV. OPTIMIZATION RESULTS

The modified PSO algorithm is used to optimize the beamforming weights. The goals of this optimization are to minimize the SLLs, maximize the matching between copolar beams, and create a null at 90° degrees away from the boresight of each quadrant radiation pattern. This way we have the minimum interference between radiation patterns of adjacent quadrants. Therefore, the optimization problem is defined as:

$$\begin{aligned} \underset{w}{\text{Minimize}} \quad & P_{i_{H,V}}\left(\varphi_i = \varphi_{0_i} \pm 90^\circ\right) \\ \text{Subject to} \quad & SLL_{i_{H,V}} < SLL_{th}, \\ & BW_{i_{H,V}} < BW_{th}, \\ & ME_i \approx 0, \quad i = 1, \ldots, 4 \end{aligned}$$

where w stands for the beamforming weights, $SLL_{H,V}$ is the SLLs for horizontal and vertical polarizations compared to the mask, φ_{0_i} is the i^{th} main beam direction (i.e., 0°, 90°, 180°, 270°), and P_i is the power of i^{th} radiation pattern in φ_i direction. ME_i is the mismatch error between copolar patterns and is defined as the difference between copolar beams of the H- and V-polarized beams. The mismatch between patterns in the vertical or horizontal plane can cause inaccurate weather observations. ME_i is defined as:

$$ME_i \triangleq \sum_N |P_{\text{h}} - P_{\text{v}}| \tag{6}$$

For the polarimetric weather sensing, it is required to have a mismatch error of less than 0.1dB to achieve accurate dual-polarization weather measurements.

Fig. 6 shows the optimized radiation pattern for 2m-, 5m-, and 10m-CPPAR with dipole elements compared to the patch design. It can be seen from this figure that the dipole elements yield lower SLLs and lower backlobs compared to the patch elements. For horizontal polarization with the patch antenna, the backlobe levels of 2-, 5-, and 10m-CPPAR size, are around −33dB, −38dB, and −50dB, and with dipole antennas are around −40dB, −66dB, and −75dB, respectively. It can be seen from Fig. 6 that the MPSO optimization for 5m-, and 10m-CPPAR dipole element design can achieve desired nulls to reduce the interference effects. As can be seen from Fig. 6b,c, it is more efficient to use dipole antennas with at least 10dB lower backlobe level, compared to patch antennas. Also, the radiation patterns of the 5m-CPPAR, and 10m-CPPAR have lower than −60dB nulls on ±90° and 180° degrees, which offers lower interference between radiation patterns of adjacent quadrants.

The optimized radiation patterns are compared to Taylor distribution (4, −30), and the results for H-pol with dipole antennas are shown in Fig. 7. It can be seen from Fig. 7b that two acceptable nulls are achieved by the proposed MPSO algorithm (i.e., −68dB, and −76dB) on ±90°, with 17dB and 24dB lower levels compared to the Taylor distribution. Fig. 7c shows the radiation patterns for 10m-CPPAR with around −77dB, and −78dB nulls on ±90° degrees for H-pol, which are at least 24dB less than Taylor distribution. It should be noted that the null steering on ±90° is more sensitive to the phase of beamforming weights rather than their amplitude. This figure also shows that our proposed MPSO algorithm can achieve at least 6dB improvement in SLLs compared to Taylor distribution with the same beamwidth.

The BW, SLLs, and the null levels for both H-pol and V-pol are presented in Table 1. The BWs for 2m-CPPAR are around 4° and for 5m- and 10m-CPPAR sizes are around 2°, and 1°, respectively. It is normally expected that the beamwidth decreases as either the number of elements or the spacing between them increase. The element spacing in the horizontal plane is selected to be 0.58λ. The beamwidth could also be reduced at the cost of increasing the sidelobe levels. However, the optimization goal is to steer two nulls on ±90° subject to achieve relatively low SLLs while matching all copolar beams. Also, the optimization is supposed to achieve the same BWs for all four concurrent beams, and for both H- and V- polarizations to minimize the mismatch error not only between H- and V-polarizations but also between

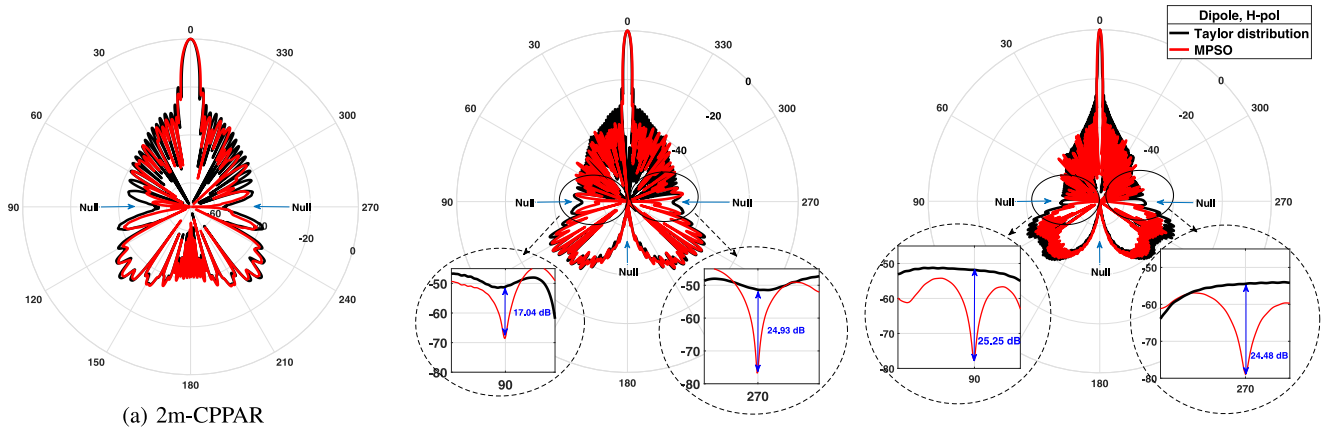

(a) 2m-CPPAR (b) 5m-CPPAR (c) 10m-CPPAR

FIGURE 7. MPSO optimized radiation patterns for a) 2m-CPPAR, b) 5m-CPPAR, and c) 10m-CPPAR using the proposed crossed dipole antenna compared to Taylor distributions.

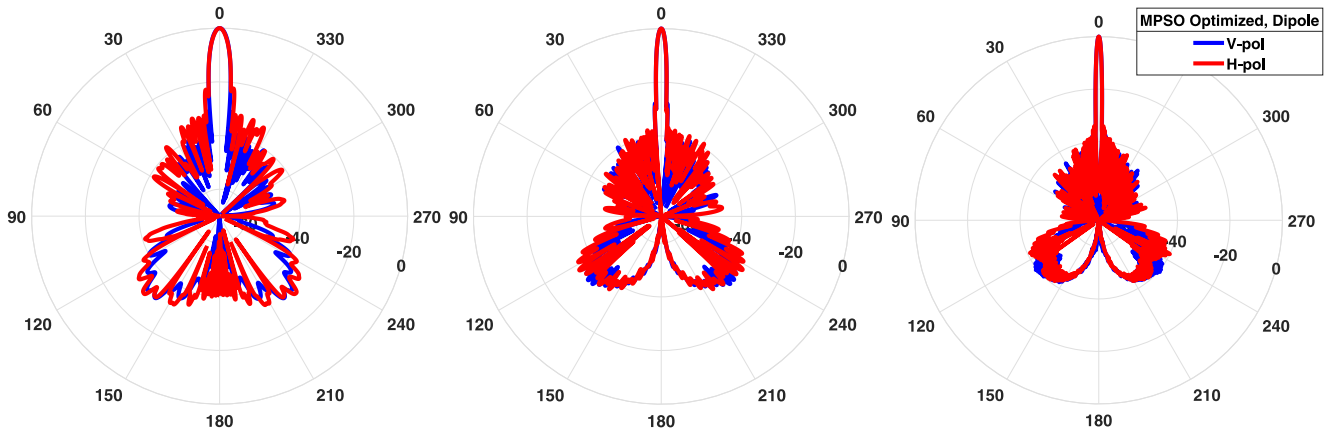

(a) 2m-CPPAR (b) 5m-CPPAR (c) 10m-CPPAR

FIGURE 8. MPSO optimized radiation patterns for H- pol and V-pol for a) 2m-CPPAR, b) 5m-CPPAR, and c) 10m-CPPAR using the proposed crossed dipole antenna.

TABLE 1. Beam characteristics (sidelobe level, beam width, null levels) for different CPPAR size, polarization and antenna type.

	2m-CPPAR				5m-CPPAR				10m-CPPAR			
Antenna type	Patch		Dipole		Patch		Dipole		Patch		Dipole	
Polarization	H-pol	V-pol	H-pol	V-pol	H-pol	V-pol	H-pol	V-pol	H-pol	V-pol	H-pol	V-pol
SLL, dB	-21.98	-25.23	-22.65	-30.85	-21.75	-24.11	-28.97	-27.81	-33.19	-34.57	-35.08	-34.38
BW, degree	4.01	4.01	4.03	4.03	1.95	1.95	1.95	1.95	1.04	1.04	1.04	1.04
90-degree Null, dB	-67.6	-56.45	-68.05	-64.78	-59.65	-60.47	-68.16	-69.23	-60.96	-69.70	-77.76	-78.10
270-degree Null, dB	-59.12	-55.27	-68.03	-70.01	-54.38	-63.44	-76.32	-74.28	-61.21	-69.08	-78.98	-79.81
180-degree Null, dB	-33.46	-44.75	-40.31	-55.63	-38.54	-60.90	-66.45	-69.21	-50.11	-66.83	-75.71	-78.11

different beam patterns, which can cause inaccurate weather observations, especially for commutating beam scan.

The SLLs for both H- and V-polarizations are also presented in Table 1. The SLLs for 2m-CPPAR with patch elements are around 22dB for H-pol, and around 25dB for V-pol. It can be observed that the MPSO algorithm can achieve better SLLs for CPPAR with dipole elements compared to those of patch antenna. As shown in Table 1, the V-pol generally have lower SLLs compared to H-pol. It is more difficult to optimize the H-pol compared to the V-pol, because of the ripples on the main beams for H-pol, as shown in Fig. 2a. The ripples on the main beam of the H-polarized beam are due to the higher level of coupling for H-polarized pattern compared to the V-polarized pattern, as mentioned in Section II.

The optimal beamforming weights are achieved using an evolutionary optimization algorithm which does not provide a unique solution to the optimization problem [28]. The MPSO algorithm is performed to optimize the beamforming weights of all elements. It is clear that the presented multi-objective optimization problem causes an asymmetrical current distribution, and it will not affect the practical implementation [28]. In the case of practical limitations, the smooth amplitude distribution can be achieved by adding

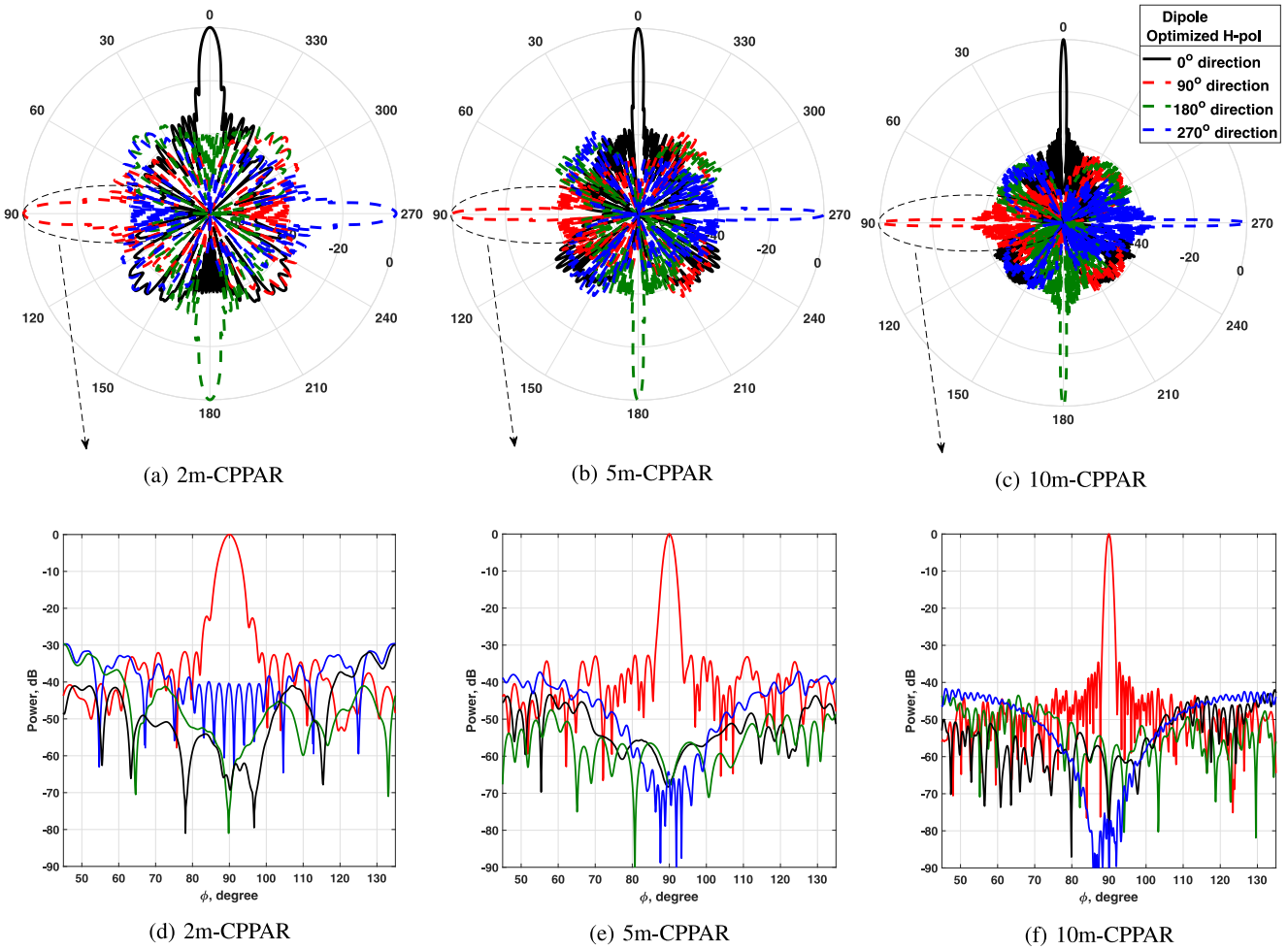

(a) 2m-CPPAR (b) 5m-CPPAR (c) 10m-CPPAR

(d) 2m-CPPAR (e) 5m-CPPAR (f) 10m-CPPAR

FIGURE 9. Optimized radiation pattern for a,d) 2m-CPPAR, b,e) 5m-CPPAR, and c,f) 10m-CPPAR.

another constraint to the optimization problem. However, it may reduce the solution space of the optimization problem and reduce its degree of freedom.

Fig. 8 shows the optimized radiation patterns for the CPPAR with dipole antennas for H-polarization and V-polarization. It is required to achieve a mismatch error of less than 0.1dB, for the accurate polarimetric weather sensing. As can be seen from Fig. 8, the main beam of H-pol and V-pol patterns are entirely matched by the proposed MPSO optimization. The mismatch between the copolar beams could reduce the correlation between horizontal and vertical polarized beams and could result in inaccurate weather sensing, especially for the polarimetric parameters such as copolar cross-correlation coefficient ρ_{hv} [5].

Fig. 9 shows the concurrent radiation patterns for the 2m-, 5m- and 10m-CPPAR. Four dual-polarized beams simultaneously scan the 360-degree in azimuth to provide faster data updates for the radar system. The main beam on 90^o direction and the achieved nulls of other beams in this direction are shown in Fig. 9d, e, f. It is shown that as the radius of the cylinder increases, the sharper nulls are achieved, and thus, less interference can be achieved. For the 10-m CPPAR the nulls levels reach below -70dB compared to the peak of the main beam showing a substantial amount of independency between the concurrent beams.

It can be seen from Fig. 9a,d that the backlobe level for the 2m-CPPAR using dipole antennas is around -40dB, which results in destructive interference to adjacent beams. The backlobe level for the 2m-CPPAR using patch antenna for H-polarization is around -33dB as shown in this figure and Table 1. Fig. 9b shows the four radiation patterns for the 5m-CPPAR. The backlobe level for the 5m-CPPAR using patch antenna is around -38dB for H-pol and for CPPAR with dipole elements is around -66dB, which are acceptable to be used for the radar system. The radiation patterns for the 10m-CPPAR is shown in Fig. 9c,f, and the backlobe level using dipole antennas is around -75dB compared to the patch antenna with around -50dB. It can be observed that the desired nulls are achieved for the 10m-CPPAR with dipole elements. Therefore, a 10m-CPPAR system with dipole elements is destined with the desired radiation patterns with low SLLs and matched co-polarization patterns, and the proposed adaptive null steering technique can be used to mitigate the interference among the concurrent beams. It is presented in

Table 1 that the MPSO can achieve at least −75dB nulls for 10m-CPPAR with dipole antenna compared to at least −66dB for 5m-CPPAR and −40dB for 2m-CPPAR.

V. CONCLUSION

In this article, we have proposed a beamforming optimization technique to achieve a radar system that can provide fast data updates using the conformal phased array radar system. Seeking the optimized pattern, we followed two parallel approaches in both the element scale and the array scale. In the element scale, we have proposed a cylindrical crossed dipole phased array antenna and demonstrated its feasibility through simulation and experiments. Surface wave suppression and lower coupling between elements, as demonstrated in the proposed crossed dipole's active element pattern, simplify achieving the optimized pattern. A modified PSO algorithm was proposed to optimize the beamforming weights of CPPAR antennas to achieve the radiation pattern with low sidelobe levels, desired beamwidth, and highly matched copolar patterns. To achieve fast data updates for severe weather observations, a radar system was proposed to transmit multi-scanning beams in each 90-degree sector of CPPAR. The interference between adjacent beams was mitigated by using a novel adaptive nulling technique. CPPAR pattern synthesis was presented for different CPPAR sizes (i.e., 2m, 5m, and 10m) using the crossed dipole and patch antennas. The proposed crossed dipole cylindrical array can benefit weather surveillance through its fast data update and precise polarimetric performance.

REFERENCES

[1] G. Zhang, R. D. Palmer, D. S. Zmic, and R. J. Doviak, "Cylindrical polarimetric phased array radar," U.S. Patent 8 988 274, Mar. 24, 2015,

[2] M. E. Weber, J. Y. Cho, J. M. Flavin, J. S. Herd, and M. M. Vai, "Multi-function phased array radar for U.S. civil-sector surveillance needs," in *Proc. 32nd Conf. Radar Meteorol. Albuquerque*, Oct. 2005.

[3] H. Saeidi-Manesh, M. Mirmozafari, and G. Zhang, "Low cross-polarisation high-isolation frequency scanning aperture coupled microstrip patch antenna array with matched dual-polarisation radiation patterns," *Electron. Lett.*, vol. 53, no. 14, pp. 901–902, 2017.

[4] D. S. Zrnić, A. Ryzhkov, J. Straka, Y. Liu, and J. Vivekanandan, "Testing a procedure for automatic classification of hydrometeor types," *J. Atmos. Ocean. Technol.*, vol. 18, no. 6, pp. 892–913, 2001.

[5] M.-H. Golbon-Haghighi, G. Zhang, and R. J. Doviak, "Ground clutter detection for weather radar using phase fluctuation index," *IEEE Trans. Geosci. Remote Sens.*, vol. 57, no. 5, pp. 2889–2895, May 2019.

[6] G. Zhang, R. J. Doviak, D. S. Zrnić, R. Palmer, L. Lei, and Y. Al-Rashid, "Polarimetric phased-array radar for weather measurement: A planar or cylindrical configuration?" *J. Atmos. Ocean. Technol.*, vol. 28, no. 1, pp. 63–73, 2011.

[7] J. E. Stailey and K. D. Hondl, "Multifunction phased array radar for aircraft and weather surveillance," *Proc. IEEE*, vol. 104, no. 3, pp. 649–659, Mar. 2016.

[8] D. S. Zrnic *et al.*, "Agile-beam phased array radar for weather observations," *Bull. Amer. Meteorol. Soc.*, vol. 88, no. 11, pp. 1753–1766, 2007.

[9] Z. Li, G. Zhang, M.-H. Golbon-Haghighi, H. Saeidi-Manesh, M. Herndon, and H. Pan, "Initial observations with electronic and mechanical scans using a cylindrical polarimetric phased array radar," *IEEE Geosci. Remote Sens. Lett.*, vol. 18, no. 2, pp. 271–275, Feb. 2021.

[10] G. Zhang, *Weather Radar Polarimetry*. Boca Raton, FL, USA: CRC Press, 2016.

[11] S. Karimkashi and G. Zhang, "A dual-polarized series-fed microstrip antenna array with very high polarization purity for weather measurements," *IEEE Trans. Antennas Propag.*, vol. 61, no. 10, pp. 5315–5319, Oct. 2013.

[12] D. M. Pozar, *Microwave Engineering*. Hoboken, NJ, USA: Wiley, 2009.

[13] J. Sureau and A. Hessel, "Element pattern for circular arrays of axial slits on large conducting cylinders," *IEEE Trans. Antennas Propag.*, vol. 17, no. 6, pp. 799–803, Nov. 1969.

[14] J.-C. Sureau and A. Hessel, "Element pattern for circular arrays of waveguide-fed axial slits on large conducting cylinders," *IEEE Trans. Antennas Propag.*, vol. 19, no. 1, pp. 64–74, Jan. 1971.

[15] C. J. Fulton and A. Mirkamali, "A computer-aided technique for the analysis of embedded element patterns of cylindrical arrays [em programmer's notebook]," *IEEE Antennas Propag. Mag.*, vol. 57, no. 3, pp. 132–138, Jun. 2015.

[16] M. Mirmozafari, H. Saeidi-Manesh, and G. Zhang, "Highly isolated crossed dipole antenna with matched copolar beams," *Electron. Lett.*, vol. 54, no. 8, pp. 470–472, 2018.

[17] M. Mirmozafari, G. Zhang, C. Fulton, and R. J. Doviak, "Dual-polarization antennas with high isolation and polarization purity: A review and comparison of cross-coupling mechanisms," *IEEE Antennas Propag. Mag.*, vol. 61, no. 1, pp. 50–63, Feb. 2019.

[18] J. D. Díaz *et al.*, "A cross-stacked radiating antenna with enhanced scanning performance for digital beamforming multifunction phased-array radars," *IEEE Trans. Antennas Propag.*, vol. 66, no. 10, pp. 5258–5267, Oct. 2018.

[19] H. Saeidi-Manesh and G. Zhang, "High-isolation, low cross-polarization, dual- polarization, hybrid feed microstrip patch array antenna for MPAR application," *IEEE Trans. Antennas Propag.*, vol. 66, no. 5, pp. 2326–2332, May 2018.

[20] M. Mirmozafari, S. Saeedi, G. Zhang, and Y. Rahmat-Samii, "A crossed dipole phased array antenna architecture with enhanced polarization and isolation characteristics," *IEEE Trans. Antennas Propag.*, vol. 68, no. 6, pp. 4469–4478, Jun. 2020.

[21] M.-H. Golbon-Haghighi, H. Saeidi-Manesh, G. Zhang, and Y. Zhang, "Pattern synthesis for the cylindrical polarimetric phased array radar (CPPAR)," *Progr. Electromagn. Res.*, vol. 66, pp. 87–98, Mar. 2018.

[22] R. J. Mailloux, *Phased Array Antenna Handbook*, Artech House, Inc., Norwood, MA, USA, 2005.

[23] S. Karimkashi and G. Zhang, "An optimal design of a cylindrical polarimetric phased array radar for weather sensing," *Radio Sci.*, vol. 47, no. 2, pp. 1–10, 2012.

[24] J. O. Yang, Q. R. Yuan, F. Yang, H. J. Zhou, Z. P. Nie, and Z. Q. Zhao, "Synthesis of conformal phased array with improved NSGA-II algorithm," *IEEE Trans. Antennas Propag.*, vol. 57, no. 12, pp. 4006–4009, Dec. 2009.

[25] J. H. Holland, "Genetic algorithms," *Sci. Amer.*, vol. 267, no. 1, pp. 66–73, 1992.

[26] D. W. Boeringer and D. H. Werner, "Efficiency-constrained particle swarm optimization of a modified bernstein polynomial for conformal array excitation amplitude synthesis," *IEEE Trans. Antennas Propag.*, vol. 53, no. 8, pp. 2662–2673, Aug. 2005.

[27] D. W. Boeringer and D. H. Werner, "Particle swarm optimization of a modified bernstein polynomial for conformal array excitation synthesis," in *Proc. IEEE Antennas Propag. Soc. Symp.*, vol. 3, 2004, pp. 2293–2296.

[28] S. Karimkashi and G. Zhang, "Optimizing radiation patterns of a cylindrical polarimetric phased-array radar for multimissions," *IEEE Trans. Geosci. Remote Sens.*, vol. 53, no. 5, pp. 2810–2818, May 2015.

[29] R. Eberhart and J. Kennedy, "A new optimizer using particle swarm theory," in *Proc. 6th Int. Symp. Micro Mach. Human Sci.*, 1995, pp. 39–43.

[30] R. C. Eberhart, Y. Shi, and J. Kennedy, *Swarm Intelligence*. Amsterdam, The Netherlands: Elsevier, 2001.

[31] J. Kennedy, "Particle swarm optimization," *Encyclopedia of Machine Learning*. Boston, MA, USA: Springer, 2010, pp. 760–766.

[32] M. Khodier and M. Al-Aqeel, "Linear and circular array optimization: A study using particle swarm intelligence," *Progr. Electromagn. Res.*, vol. 15, pp. 347–373, Jun. 2009.

MOHAMMAD-HOSSEIN GOLBON-HAGHIGHI (Member, IEEE) received the B.Sc. degree in electrical engineering from the Shiraz University of Technology, Shiraz, Iran, in 2009, and the M.Sc. degree in electrical engineering from the K. N. Toosi University of Technology, Tehran, Iran, in 2012, and the Ph.D. degree in electrical and computer engineering from the University of Oklahoma, Norman, OK, USA, in 2019. He is currently a Postdoctoral Research Fellow with the Advanced Radar Research Center. His research interests include radar signal processing, estimation and detection, pattern recognition, and polarimetric phased array radars. He was a recipient of several awards, including the prestigious Gallogly College of Engineering Dissertation Excellence Award, the William Barkow Scholarship, and the Farrow Endowment Scholarship for his outstanding academic achievements, at the University of Oklahoma. He is a member of the IEEE Signal Processing Society and the IEEE Geoscience and Remote Sensing Society.

MIRHAMED MIRMOZAFARI (Member, IEEE) received the B.S. degree in electrical engineering from the University of Guilan, Rasht, Iran, in 2008, the M.S. degree in telecommunications engineering from the University of Urmia, Urmia, Iran, in 2011, and the Ph.D. degree in electrical engineering from the University of Oklahoma, Norman, OK, USA, in 2018. From 2011 to 2014, he was a Senior RF Engineer with the Pattern Research Laboratory, Tehran, Iran. From 2014 to 2018, he was a Research Assistant with the Advanced Radar Research Center, University of Oklahoma, where he still holds an affiliate position. In 2018, as a Postdoctoral Research Associate he joined the Department of Electrical and Computer Engineering, University of Wisconsin–Madison, Madison, WI, USA, where he is currently an Assistant Scientist. His research interests include applied electromagnetic, antenna design, polarimetric phased array radars, additive manufacturing, vacuum electronics, and high power microwave. He received the Second Prize Student Paper Award at IEEE APS/URSI 2018 Conference, and was also featured author of *Electronic Letters*, issue 8, volume 54, 2018. He is a member of the IEEE ANTENNAS AND PROPAGATION and the IEEE Microwave Theory and Techniques Societies, and he serves as a technical reviewer for several IEEE publications.

HADI SAEIDI-MANESH (Member, IEEE) received the B.S. and M.S. degrees in electrical engineering (electromagnetics) from the K. N. Toosi University of Technology, Tehran, Iran, in 2010 and 2012, respectively, and the Ph.D. degree in electrical and computer engineering (electromagnetics) from the University of Oklahoma, Norman, OK, USA, in 2019, where he was a Postdoctoral Research Fellow with the Advanced Radar Research Center from 2019 to 2020. In 2020, he joined Metawave Corporation, Carlsbad, CA, USA, where he is currently a Staff Antenna and Hardware Engineer. His research interests include the area of antenna arrays, polarimetric phased array radars, and mm-wave phased array antennas. He is a member of the IEEE Antenna and Propagation Society.

GUIFU ZHANG (Senior Member, IEEE) received the B.S. degree in physics from Anhui University in 1982, the M.S. degree in radio physics from Wuhan University in 1985, and the Ph.D. degree in electrical engineering from the University of Washington in 1998.

He was an Assistant Professor and an Associate Professor with the Space Physics Department, Wuhan University from 1985 to 1993. In 1989, he worked as a Visiting Scholar with the Communication Research Laboratory, Tokyo, Japan. From 1993 to 1998, he studied and worked with the Department of Electrical Engineering, University of Washington, where he was first a Visiting Scientist and later a Ph.D. student. He was a Scientist with the National Center for Atmospheric Research, Boulder, CO, USA, from 1998 to 2005. In 2005, he joined the School of Meteorology, University of Oklahoma, where he is currently a Professor. He formulated theories of phased array weather radar interferometry and polarimetry. He has authored *Weather Radar Polarimetry* and published over 100 journal papers for his research work in radar theory/technology, signal processing, and applications in meteorology and hydrology. He led the development of advanced signal processing algorithm to improve weather radar data quality and of the polarimetric radar data simulators to bridge the gap between radar meteorology and numerical weather prediction. Among his current projects, he is working on topics, such as the optimal use of polarimetric radar data in quantitative precipitation estimation and quantitative precipitation forecast and the research and development of polarimetric phased array radars for weather measurements and multimission capability.

Prof. Zhang has received five U.S. patent awards and filed over ten intellectual property disclosures. He also received several research and excellent paper awards.